microorganisms

MDPI

Article

Innovative embedding method for fast electron microscopy examination of virus culture: application to SARS-CoV-2

Marion Le Bideau1, Nathalie Wurtz1,2, Jean-Pierre Baudoin1*, Bernard La Scola1,2*

[1] Microbes, Evolution, Phylogeny and Infection (MEPHI), UM63, Institut de Recherche pour le Développement (IRD), Assistance Publique - Hôpitaux de Marseille (AP-HM), Aix-Marseille University, Marseille, France;

[2] IHU Méditerranée Infection, Marseille, France;

* Corresponding authors: Dr. Jean-Pierre Baudoin and Prof. Bernard La Scola, Microbes, Evolution, Phylogeny and Infection (MEPHI), UM63, Institut de Recherche pour le Développement (IRD), IHU Méditerranée Infection, Assistance Publique - Hôpitaux de Marseille (AP-HM), Aix-Marseille University, 19-21 boulevard Jean Moulin, 13005 Marseille, France: jpbaudoin@live.fr; bernard.la-scola@univ-amu.fr

Abstract: Despite the development of new diagnostic methods, co-culture, based on sample inoculation of cell monolayers coupled with electron microscopy (EM) observation, remains the gold-standard in virology. Indeed, co-culture allows for the study of cell morphology (infected and not infected), the ultrastructure of the inoculated virus and the different steps of the virus infectious cycle. Most EM methods for studying virus cycles are done after infected cells are produced in large quantities and detached to obtain a pellet. Here, cell culture was performed in sterilized, collagen-coated single-break strip wells. After one day in culture, cells were infected with Sars-CoV-2. Wells of interest were fixed at different time points, from 2 to 36 hours post-infection. Microwave-assisted resin embedding was accomplished directly in the wells in 4 hours. Finally, ultra-thin sections were cut directly through the infected-cell monolayers. Our methodology requires in total less than 4 days for preparing and observing cells. Furthermore, by observing undetached infected cell monolayers, we were able to observe new ultrastructural findings such as cell-cell interactions and baso-apical cellular organization related to the virus infectious cycle. Our innovative methodology thus not only saves time for preparation but also adds precision and new knowledge about viral infection, as shown here for SarS-CoV-2

Keywords: SARS-CoV-2; electron microscopy; embedding method; microwaves; single-break strip.

Citation: Lastname, F.; Lastname, F.; Lastname, F. Title. *Microorganisms* **2021**, *9*, x. https://doi.org/10.3390/xxxxx

Academic Editor: Firstname Lastname

Received: date
Accepted: date
Published: date

1. Introduction

Electron microscopy (EM) in biology is a powerful tool for examining the morphology and ultrastructure of cells. In the virology field, EM examination of viruses grown in cultured cells has been a key tool in determining the etiologic agent in numerous disease outbreaks caused by previously unknown viruses, and remains the gold standard for understanding cellular virus infectious cycles [1–5]. Besides resolving difficulties in differentiating viruses from subcellular structures [6], EM examination of viruses grown in cultured cells provides visualization of the different steps of the viral life cycle (attachment, entry, replication, assembly and egress) and the study of the ultrastructure of the virus and infected cell [7,8].

The standard methodology for accessing the ultrastructure of virus-infected cells in culture is to produce a large amount of infected cells, chemically- or cryo-fix the cells and then resin-embed the cells [8]. Generally, resin embedding of fixed cells is achieved after mechanical or trypsin detachment of the cells from the substrate and pelleting of the cells. Ultramicrotomy is performed on the pellet and observations are made on heavy-metal contrasted ultra-thin sections by transmission or scanning electron microscopy. Overall, this approach is time-consuming (~ three weeks), and provides images of

rounded, detached cells. The cells at the most advanced stage of infection are very fragile and typically burst during preparation. Another limitation is the requirement of relatively large culture volumes for obtaining a concentrated cell pellet.

Infected cultured cells can also be prepared for EM as monolayers via flat embedding. Cell monolayers can be grown on flat supports such as glass or plastic coverslips (for chemical fixation), sapphire discs (for high-pressure freezing) or on EM grids (for cryo-EM) [8]. Flat embedding of cell monolayers and plane sectioning of the cells, with cutting plane parallel to the substrate, has proven a powerful method for accessing information about the ultrastructure of cells grown in two dimensions (2D), especially for migrating cells [9]. In the field of virology, flat embedding and plane sectioning of virus infected cells has been used in only a few studies, for example with cells grown on ACLAR embedding films [10], or with cells grown on gridded slides for correlative light-electron-microscopy studies [11].

Here, we developed a novel approach for EM after in-well flat embedding and plane sectioning of virus-infected cells, using breakable cell culture dishes and microwave EM processing. Our approach can be broadly used for fast infectious cycle monitoring by EM, providing images of undetached cell monolayers at selected time points. Our relatively simple method does not require any expensive equipment and can be adapted for any cytopathic effect characterized by EM and subsequent microorganism visualization and detection throughout the infectious cycle. We show here its successful use for studying the infectious cycle of Sars-CoV-2 in VeroE6 cell monolayers.

2. Materials and Methods

2.1 Cell culture and the virus infectious cycle

Substrate preparation was performed by Cell and Soft (Grenoble, France). Briefly, Greiner Bio-One 96 well single-break strip microplates (Greiner Bio-One, Frickenhausen, Germany) were UV sterilized at 365 nm for 5 minutes (UV-KUB 1, Kloé, France), (125 mW/cm^2) under a laminar flow hood. Collagen coating was then performed under a sterile laminar flow cabinet. Subsequently, 400 ng of rat tail Collagen I (Corning life science, Amsterdam, The Netherlands) was added to each well and incubated at 37°C overnight. Plates were stored at 4°C until use at our laboratory. Vero E6 cells were suspended at 2.10^5 cells/mL in MEM supplemented with 10% fetal calf serum and 1% L-glutamine (M10 medium). Then, 200 µL of this cell suspension was distributed in each modular well of two removable single-break strips (8 wells each) in a microplate and incubated for 24 hours at 37°C with 5% CO_2. Infection of Vero E6 cell monolayers was done in one of the two strips by removing culture medium and adding 50 µL of SARS-CoV-2 viral suspension (MOI of 0.1) in MEM medium supplemented with 4% fetal calf serum and 1% L-glutamine (M4 medium). The second strip was used as negative control by adding 50 µL of M4 medium only and both strips were centrifuged for 1 hour at 37°C at 2272x g. The supernatant from the wells was discarded, the cells rinsed gently three times with M4 medium and 200 µL of M4 medium was added to the 8 wells. Cells were incubated at 37°C and 5% CO_2. For each post-infection time point (2, 3, 6, 12, 18 and 36 hours), one infected and one non-infected modular well was fixed by adding 30 µL of 25% glutaraldehyde in 0.1M sodium cacodylate buffer and stored at 4°C until infectious cycle completion.

2.2 Electron Microscopy

Cells were fixed with glutaraldehyde 2.5% in 0.1M sodium cacodylate buffer. Resin embedding was microwave-assisted with a BiowavePro+ (Pelco, USA; Eloïse, France) (Table S1), by exchanging 200 µL of the different solutions at each step. Samples were washed two times with a mixture of 0.2M saccharose/0.1M sodium cacodylate and post-fixed with 1% OsO4 diluted in 0.2M Potassium hexa-cyanoferrate (III)/0.1M sodium cacodylate buffer. After two washes with distilled water, samples were gradually dehydrated by successive baths in 30%, 50%, 70%, 90%, 96% and 100% ethanol. Substitution with Epon resin (Embed 812 mixed with NMA, DDSA and DMP-30 hardener; Electron Microscopy Sciences, USA) was achieved by incubations with 25%, 50%, 75% Epon resin

in ethanol and incubations with 100% Epon resin. A final volume of 275 µL of 100% Epon resin was added to each well, and prior to microwave-curing a 3D-printed sealing cap was placed on top of the wells to protect the resin from water in the microwave polymerization chamber. Instructions for preparing sealing caps are available at the link below. Sealing caps were designed by using Autodesk Fusion 360 software. The cap file created is exported as an .stl extension file and reworked with Simplify 3D software to enter 3D print settings. The sealing caps were manufactured with Python Flex diameter 1.75 mm, a flexible thermoplastic polyurethane (TPU) filament (https://www.formfutura.com/shop/product/python-flex-2835). On Simplify 3D software, the standard properties of the Ninjaflex filament were selected: 25% filling rate, addition of a skirt composed of 3 layers and rapid printing quality (200 µm). The 3D printer used to make this cap is the 30 Pro MK2 volumic stream printer (https://www.imprimante-3d-volumic.com/en/la-gamme-imprimante-3d-detail/847-stream-30-pro-mk2.cfm). Printing is carried out continuously layer by layer. The G-Code file for this cap can be downloaded at [12]. Resin microwave-curing was performed for a total of 2 hours. All solutions used above were 0.2 µm filtered. After curing, resin blocks were manually trimmed with a razor blade and dish bottoms were detached from cell monolayers by heat-shock via immersion in liquid nitrogen for 20 s and removal of the plastic with pliers. Resin blocks were placed in a UC7 ultramicrotome (Leica), trimmed as pyramids, and ultrathin 70 nm sections were cut and placed on HR25 300 Mesh Copper/Rhodium grids (TAAB, UK). Sections were contrasted according to Reynolds [13]. Grids were attached to double-side tape on a glass slide and platinum-coated at 10mA for 20 s with a MC1000 sputter coater (Hitachi). Electron micrographs were obtained on a SU5000 SEM (Hitachi High-Technologies, HHT, Japan) operated in high-vacuum at 7 kV accelerating voltage and observation mode (spot size 30) with BSE detector, and magnifications ranging from x1,500 to x40,000.

3. Results

The total processing time for resin-embedding was 4 hours, from the first fixative wash to cured resin blocks. For curing resin with microwaves, the culture wells needed to be closed, as wells were placed in water, and a 3D-printed cap was placed on top of the well to guarantee sealing. An extra day was needed for resin block extraction from the plastic wells and ultramicrotomy, and one final day was employed for ultra-thin section contrast with heavy metals and image acquisitions by SEM. Thus, for the Sars-CoV-2 infectious cycle examination by EM, a total of 3.5 processing days was needed, from cell culture to observation, plus three days for the infectious cycle to occur. The entire process is described in Figure 1.

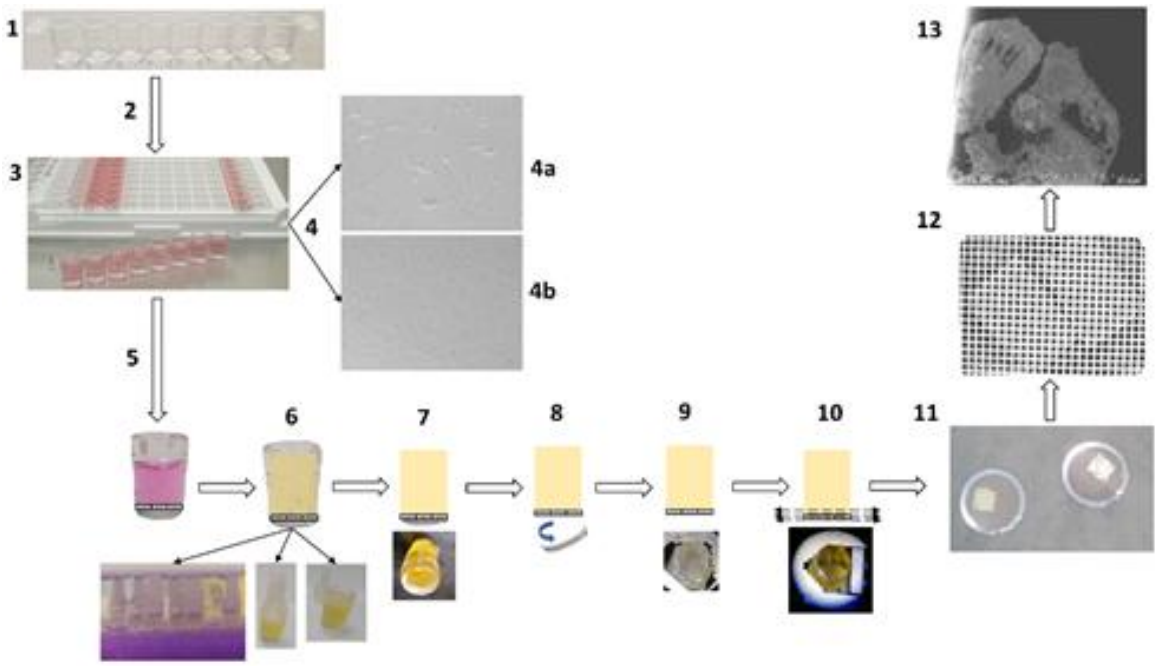

Figure 1. Schematic representation of methodology for fast electron microscopic examination of virus culture. (1) Removable single-break strips are UV sterilized and collagen-coated. (2) Cell culture with 200 µL suspensions of Vero E6 cells at 2.105 cells/mL per well. (3) Cells are virus-inoculated with 50 µL of strains or clinical sample per well. (4) Cytopathic effect detection: cytopathic effect (4a) is monitored by bright-field light microscopy, with comparison to negative control (4b). (5) Cell fixation: cell monolayers are fixed with 2.5% final glutaraldehyde. (6) In-well resin embedding in 4 hours: washes, dehydration, resin substitution and wells closed by cap sealing for microwave polymerization. (7) Plastic pruning: resin blocks are manually trimmed with a razor blade. (8) Detachment of cell monolayer: the plastic bottom of the well is detached by heat-shock via immersion in liquid nitrogen for 20 s. (9) Resin block: the resin block containing the cell monolayer at one side is ready for ultramicrotomy. (10) Ultramicrotomy: the resin block is trimmed as a pyramid and ultra-thin sections are obtained. (11) Positioning on grids: ultra-thin sections are deposited on copper/rhodium grids. (12) Contrast and metal deposition: sections are contrasted with uranyl acetate and lead citrate and grids attached to a glass slide are platinum sputter-coated. (13) Electron microscopy: electron micrographs are obtained by SEM.

With our innovative approach, we observed previously described features of the Sars-CoV-2 infectious cycle, highly comparable to that of SARS-CoV (Figures 2-6): neo-virions formed in the peri-nuclear region from a budding of the endoplasmic reticulum-Golgi apparatus complex at the level of morphogenesis matrix vesicae, and new particles were expelled from the cells through cell lysis or by fusion of virus-containing vacuoles with the cell plasma membrane [14–20]. Our approach also provided new ultrastructural insights into the Sars-CoV-2 infectious cycle in Vero E6 cells. Indeed, our ability to observe sections of intact cell monolayers instead of pelleted cells showed both the relationships between cells, such as cell-cell contacts, and the characteristics of each single cell at different levels along a cellular baso-apical axis. Cells could be seen touching each other i) along large plasma membrane regions, with velcro-like membrane appositions resembling adherens junctions (Figures 2A,C); ii) at discrete locations with electron-dense contacts resembling tight junctions (Figures 3D,E;4D-F); or iii) interconnecting microvilli (Figures 4E,I; 5E-H). Large cellular protrusions could be seen (Figures 3A,B), potentially enwrapping neighboring cells (Figures 4A,B). Cellular protrusions appeared more frequently as post-infection time progressed, with mostly spherical or triangular cells at early time points and ultimately asymmetric cells with numerous protrusions. We found filopodia containing actin microfilaments and presenting the characteristic V-shape at their base (Figures 6A,B). These filopodia were devoid of virion particles, either internally or on the surface. The filopodia were different from the numerous I-shaped microvilli (mean diameter 90 ±30 nm, n=21), characteristic of epithelial Vero E6 cells (Figures 3D-I;4D-I;5). Microvilli were present in basolateral cellular regions between more or less distant cells and in regions located more apically in the cells. Microvilli were enriched at their surface with mature Sars-CoV-2 virions, especially from 12hpi. Strikingly, microvilli of neighboring cells could be seen intermingled, with an amount of virion particles proportional to the number of villi. While we had already observed the canalicular system of Vero E6 cells and its content in Sars-CoV-2 virions, this tubular and interconnected vacuoles system was more pronounced using our approach (Figures 4G-I;6C-F). We observed networks of tubules and compartments that ultimately connected to the external plasma membrane, mostly in apical cellular regions. The Sars-CoV-2-rich compartments connected to the canalicular system were smaller in diameter and less electron-dense when located closer to the plasma membrane, suggesting a progressive delivery of new virions as VMV mature and fuse with the apical tubular system.

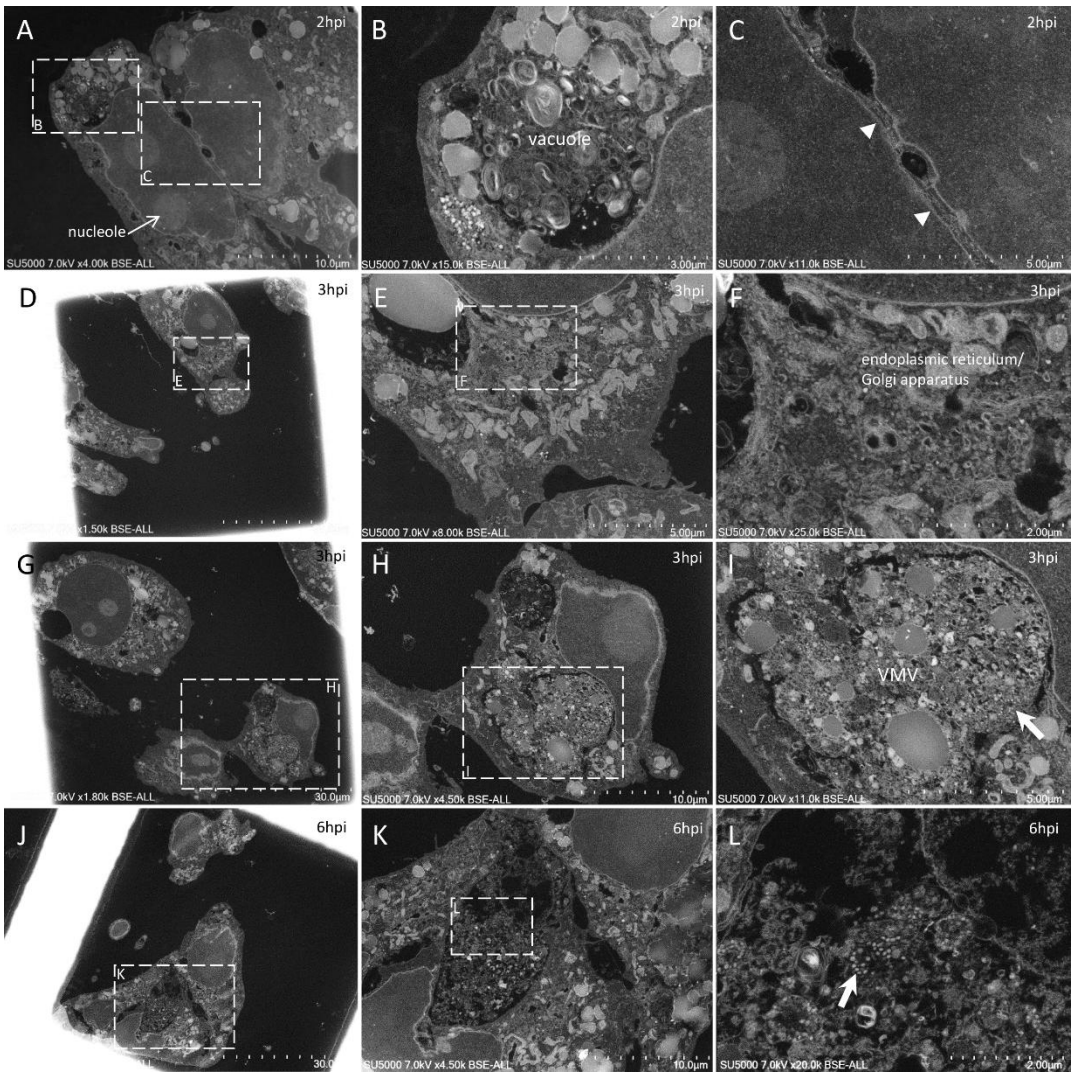

Figure 2. Ultra-thin sections of Sars-CoV-2-infected Vero E6 cells: 2hpi to 6hpi. A-C: 2hpi. Two cells (A) with plasma membranes closely associated with a 'velcro' organization (C; arrowheads). One of the two cells presents a large vacuole enriched in membranes and granules (B). D-I: 3hpi. One cell (D) presents the typical budding of the endoplasmic reticulum and Golgi apparatus compartments following Sars-CoV-2 infection (E,F). One cell (G) with a virus-morphogenesis vesicle (VMV; H,I) containing Sars-CoV-2 virions (arrow). J-L: 6hpi. A region of a lysed-cell (K) located between intact cells and containing debris and mature Sars-CoV-2 particles (L; arrow).

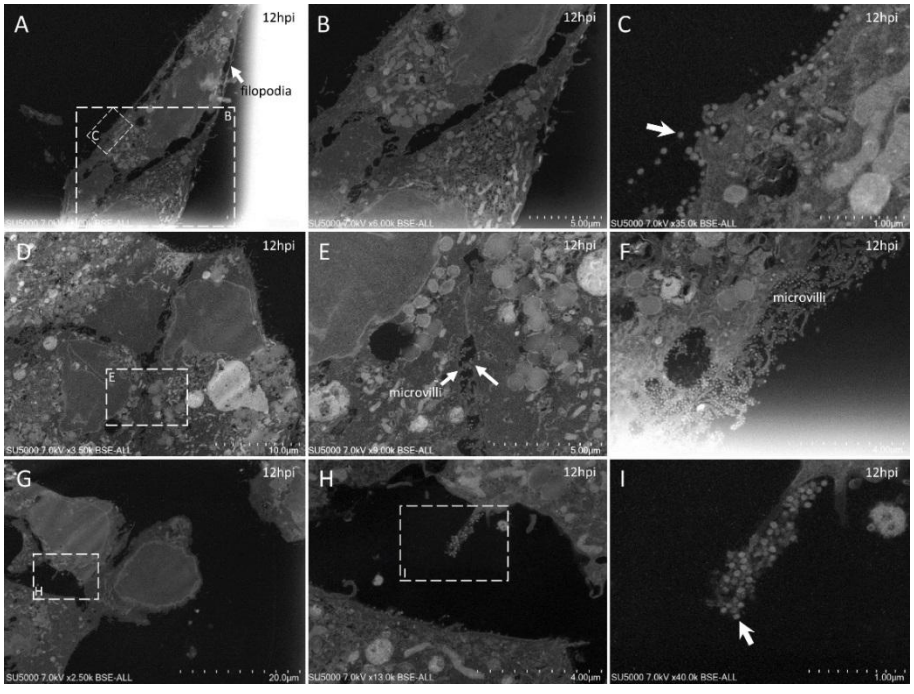

Figure 3. Ultra-thin sections of Sars-CoV-2-infected Vero E6 cells: 12hpi. A-C: two neighboring cells, one possessing a long filopodia (B) and one presenting extracellular Sars-CoV-2 particles at the plasma membrane (C; arrow). D-F: Sars-CoV-2-enriched microvilli located between neighboring cells (E) or at the cell free periphery (F). G-I: one microvillus extremely enriched in Sars-CoV-2 virions (I; arrow).

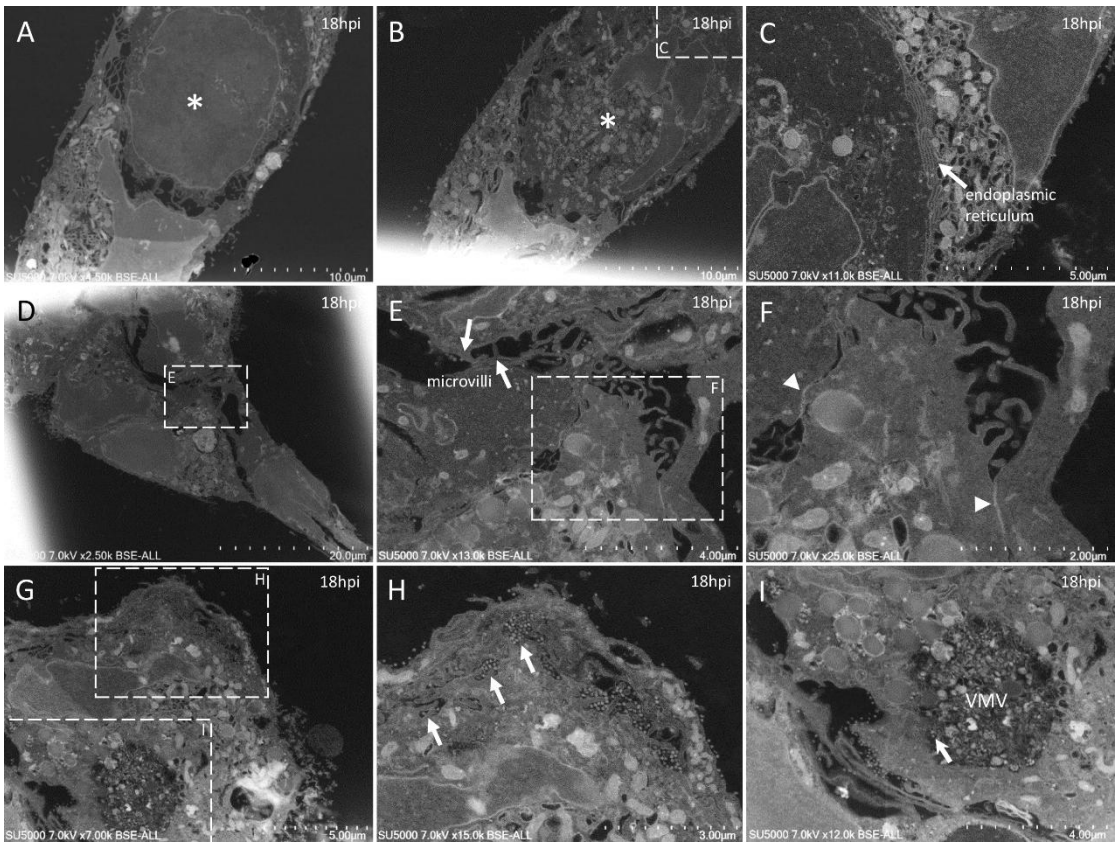

Figure 4. Ultra-thin sections of Sars-CoV-2-infected Vero E6 cells: 18hpi. A,B: two serial sections of the same cell, with cuts at the level of its nucleus (*) at different heights along its depth. In (C) the nuclear membrane/endoplasmic reticulum presents a stacked organization. D-F: adjacent cells contacting each other through microvilli (E) or electron-dense regions resembling tight junctions (F; arrowheads). G-I: Sars-CoV-2 particles (arrows) located inside a canalicular tubulo-vesicular system (H) as well as in a virus-morphogenesis vesicle (VMV; I) of the same cell.

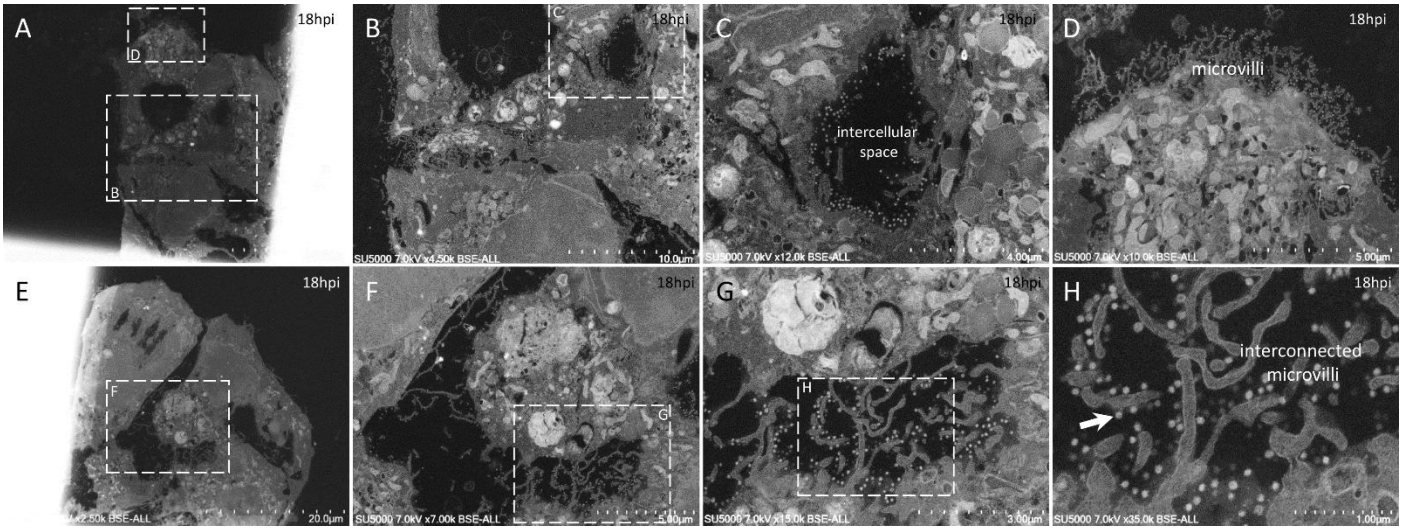

Figure 5. Ultra-thin sections of Sars-CoV-2 infected Vero E6 cells: 18hpi. A-D: neighboring cells harboring extracellular Sars-CoV-2 particles at the level of an intercellular space (C) or at the level of peripheral microvilli (D). E-H: a cellular cluster with two cells facing each other with intermingled microvilli enriched in Sars-CoV-2 particles (H; arrow).

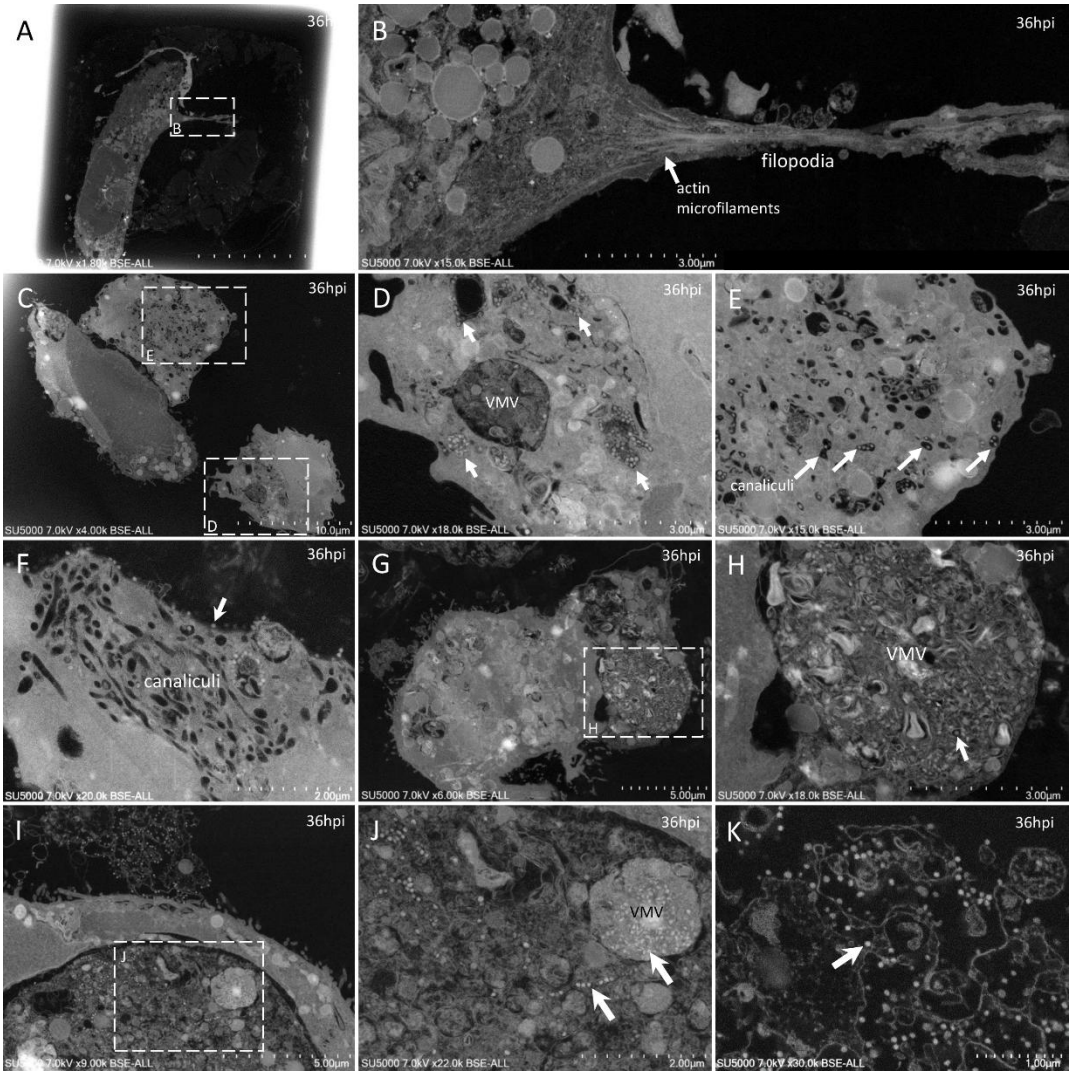

Figure 6. Ultra-thin sections of Sars-CoV-2-infected Vero E6 cells: 36hpi. A,B: a cell with a filopodia (B) containing actin microfilaments; Sars-CoV-2 virions were not detected inside such filopodia structures. C-F: cells with Sars-CoV-2 particles inside a virus-morphogenesis vesicle (VMV) or inside tubules/vesicles of the canaliculi system (D,E; arrows) or at the plasma membrane (F; arrow). G,H: large VMV containing Sars-CoV-2 virions (arrow) and membranes. I-K: in adjacent cellular regions, Sars-CoV-2 particles were found concentrated in a VMV, disseminated in a larger vacuole (J; arrows), or stitched extracellularly to the plasma membrane remnants of a lysed cell (K).

4. Discussion

Our innovative embedding method is much faster than standard methods for studying the ultrastructure of virus-infected cells. Indeed, our method saves time; initially, regarding cell culture and secondly, regarding electron microscopy. Regarding cell culture, classically three subcultures over a 6-day period are needed to obtain a pellet of infected cells. Here, with our new method that uses breakable serology microplates, cell culture prior to infection was shortened to 1 day. The use of microwaves for accelerating EM processing is a well-known technique [21–24], and its use for rapidly examining virus-infected cells proved very efficient, with EM processing duration shortened from 4.5-5.5 days with standard methods to only 4 hours. Additional experimental time for ultramicrotomy, contrast and EM observations depends on the number of wells/post-infection time-points that one is willing to analyze.

Our method also proved useful for observing unique ultrastructural cellular features of Sars-CoV-2 infection. Indeed, one advantage of our method is that it enabled the

observation of adherent undetached cells, and thus the morphological relationships between cells. For example, Sars-CoV-2-infected Vero E6 cells were seen to be interconnected by microvilli (Figures 4E,I; 5E-H). These microvilli were enriched with numerous Sars-CoV-2 particles (Figure 3F,I), as already described by our laboratory [16] and other groups [15,18,20]. We show here that not only apical microvilli were enriched in Sars-CoV-2 particles, but also intercellular baso-apical microvilli. These microvilli thus may assist the dissemination of Sars-CoV-2 particles among cells in a monolayer. Another example was the canalicular system and its content in Sars-CoV-2 virions, which was frequently observed in adherent Vero E6 cells (Figures 4G-I;6C-F), probably because cells can retain their conformation, compared to detached rounded cells in which intracellular compartments may change their spatial organization. Our images also suggested a progressive delivery of new virions as VMV mature and fuse with the apical tubular system, with Sars-CoV-2-enriched compartments connected to the canalicular system (Figures 4G-I;6C-F). Such images suggest that apical trafficking in Vero E6 cells and other Sars-CoV-2-infected epithelial cells may be of interest for pharmacological treatments to disrupt virus cell exit and viral dissemination to neighboring cells. As a complementary approach, our method provides ready-to-cut resin blocks with infected cell monolayers that are very suitable for three-dimensional (3D) reconstructions [8], by serial-block face (SBF)/focused-ion-beam(FIB)-SEM experiments [25] or manually cut serial section ribbons by TEM/SEM (Figures 4A,B) and [26].

Finally, our innovative method could be used for EM examination of any unknown infectious microorganisms, virus, or intracellular bacteria, even if only a small sample is available for infecting the cell monolayer, which can be especially useful in case of rare samples from hospitalized patients.

5. Conclusions

Our innovative embedding method provides a faster electron microscopic examination of virus-infected cells, even when a limited quantity of samples is available. As illustrated with Sars-CoV-2-infected cells, our method is also capable of revealing new ultrastructural findings, because it allows for the in-situ visualization of cell monolayers. Furthermore, our approach offers perspectives for a faster characterization of unknown viruses potentially involved in other epidemics or pandemics.

Supplementary Materials: The following are available online at www.mdpi.com/xxx/s1, Table S1: Microwave resin-embedding and polymerization settings (PELCO BioWave ProPlus).

Author Contributions: Author Contributions: Conceptualization, BLS; methodology, BLS, JPB and MLB; validation, BLS; writing—original draft preparation, JPB, NW and MLB; supervision, BLS. All authors have read and agree to the published version of the manuscript.

Funding: Part of this work was funded by a grant from the French State managed by the National Research Agency under the "Investissements d'avenir" (Investments for the Future) program under reference ANR-10-IAHU-03 (Méditerranée Infection).

Data Availability Statement: Not applicable.

Acknowledgments: We thank Jean-Christophe Sergere and Camille Migdal of Cell-Soft for their help and involvement in this work and Alain Delache for help in the design of caps.

Conflicts of Interest: The authors declare no conflicts of interest.

References

1. Fong, C.K. Electron Microscopy for the Rapid Detection and Identification of Viruses from Clinical Specimens. *Yale J Biol Med* **1989**, *62*, 115–130.
2. Roingeard, P. Viral Detection by Electron Microscopy: Past, Present and Future. *Biol Cell* **2008**, *100*, 491–501, doi:10.1042/BC20070173.

3. Goldsmith, C.S.; Miller, S.E. Modern Uses of Electron Microscopy for Detection of Viruses. *Clin Microbiol Rev* **2009**, *22*, 552–563, doi:10.1128/CMR.00027-09.
4. Laue, M. Electron Microscopy of Viruses. *Methods Cell Biol* **2010**, *96*, 1–20, doi:10.1016/S0091-679X(10)96001-9.
5. Goldsmith, C.S.; Ksiazek, T.G.; Rollin, P.E.; Comer, J.A.; Nicholson, W.L.; Peret, T.C.T.; Erdman, D.D.; Bellini, W.J.; Harcourt, B.H.; Rota, P.A.; et al. Cell Culture and Electron Microscopy for Identifying Viruses in Diseases of Unknown Cause. *Emerg Infect Dis* **2013**, *19*, 886–891, doi:10.3201/eid1906.130173.
6. Bullock, H.A.; Goldsmith, C.S.; Zaki, S.R.; Martines, R.B.; Miller, S.E. Difficulties in Differentiating Coronaviruses from Subcellular Structures in Human Tissues by Electron Microscopy. *Emerg Infect Dis* **2021**, *27*, 1023–1031, doi:10.3201/eid2704.204337.
7. Risco, C.; de Castro, I.F.; Sanz-Sánchez, L.; Narayan, K.; Grandinetti, G.; Subramaniam, S. Three-Dimensional Imaging of Viral Infections. *Annu Rev Virol* **2014**, *1*, 453–473, doi:10.1146/annurev-virology-031413-085351.
8. Romero-Brey, I.; Bartenschlager, R. Viral Infection at High Magnification: 3D Electron Microscopy Methods to Analyze the Architecture of Infected Cells. *Viruses* **2015**, *7*, 6316–6345, doi:10.3390/v7122940.
9. Baudoin, J.-P.; Viou, L.; Launay, P.-S.; Luccardini, C.; Espeso Gil, S.; Kiyasova, V.; Irinopoulou, T.; Alvarez, C.; Rio, J.-P.; Boudier, T.; et al. Tangentially Migrating Neurons Assemble a Primary Cilium That Promotes Their Reorientation to the Cortical Plate. *Neuron* **2012**, *76*, 1108–1122, doi:10.1016/j.neuron.2012.10.027.
10. Chu, H.; Wang, J.-J.; Qi, M.; Yoon, J.-J.; Wen, X.; Chen, X.; Ding, L.; Spearman, P. The Intracellular Virus-Containing Compartments in Primary Human Macrophages Are Largely Inaccessible to Antibodies and Small Molecules. *PLoS One* **2012**, *7*, e35297, doi:10.1371/journal.pone.0035297.
11. Sachse, M.; Fernández de Castro, I.; Tenorio, R.; Risco, C. The Viral Replication Organelles within Cells Studied by Electron Microscopy. *Adv Virus Res* **2019**, *105*, 1–33, doi:10.1016/bs.aivir.2019.07.005.
12. Sealing Cap File. Available Online: Https://Www.Mediterranee-Infection.Com/Acces-Ressources/Donnees-Pour-Articles/Sinnovative-Embedding-Method-for-Fast-Electron-Microscopic-Examination-of-Virus-Culture-Application-to-Sars-Cov-2/ (Accessed on 19 April 2021).
13. REYNOLDS, E.S. The Use of Lead Citrate at High PH as an Electron-Opaque Stain in Electron Microscopy. *J Cell Biol* **1963**, *17*, 208–212, doi:10.1083/jcb.17.1.208.
14. Zhu, N.; Zhang, D.; Wang, W.; Li, X.; Yang, B.; Song, J.; Zhao, X.; Huang, B.; Shi, W.; Lu, R.; et al. A Novel Coronavirus from Patients with Pneumonia in China, 2019. *New England Journal of Medicine* **2020**, *382*, 727–733, doi:10.1056/nejmoa2001017.
15. Zhu, N.; Wang, W.; Liu, Z.; Liang, C.; Wang, W.; Ye, F.; Huang, B.; Zhao, L.; Wang, H.; Zhou, W.; et al. Morphogenesis and Cytopathic Effect of SARS-CoV-2 Infection in Human Airway Epithelial Cells. *Nat Commun* **2020**, *11*, 3910, doi:10.1038/s41467-020-17796-z.
16. Brahim Belhaouari, D.; Fontanini, A.; Baudoin, J.-P.; Haddad, G.; Le Bideau, M.; Bou Khalil, J.Y.; Raoult, D.; La Scola, B. The Strengths of Scanning Electron Microscopy in Deciphering SARS-CoV-2 Infectious Cycle. *Front Microbiol* **2020**, *11*, 2014, doi:10.3389/fmicb.2020.02014.
17. Ogando, N.S.; Dalebout, T.J.; Zevenhoven-Dobbe, J.C.; Limpens, R.W.A.L.; van der Meer, Y.; Caly, L.; Druce, J.; de Vries, J.J.C.; Kikkert, M.; Bárcena, M.; et al. SARS-Coronavirus-2 Replication in Vero E6 Cells: Replication Kinetics, Rapid Adaptation and Cytopathology. *J Gen Virol* **2020**, *101*, 925–940, doi:10.1099/jgv.0.001453.
18. Eymieux, S.; Rouillé, Y.; Terrier, O.; Seron, K.; Blanchard, E.; Rosa-Calatrava, M.; Dubuisson, J.; Belouzard, S.; Roingeard, P. Ultrastructural Modifications Induced by SARS-CoV-2 in Vero Cells: A Kinetic Analysis of Viral

Factory Formation, Viral Particle Morphogenesis and Virion Release. *Cell Mol Life Sci* **2021**, *78*, 3565–3576, doi:10.1007/s00018-020-03745-y.

19. Wolff, G.; Limpens, R.W.A.L.; Zevenhoven-Dobbe, J.C.; Laugks, U.; Zheng, S.; de Jong, A.W.M.; Koning, R.I.; Agard, D.A.; Grünewald, K.; Koster, A.J.; et al. A Molecular Pore Spans the Double Membrane of the Coronavirus Replication Organelle. *Science* **2020**, *369*, 1395, doi:10.1126/science.abd3629.
20. Laue, M.; Kauter, A.; Hoffmann, T.; Möller, L.; Michel, J.; Nitsche, A. Morphometry of SARS-CoV and SARS-CoV-2 Particles in Ultrathin Plastic Sections of Infected Vero Cell Cultures. *Sci Rep* **2021**, *11*, 3515, doi:10.1038/s41598-021-82852-7.
21. Kok, L.P.; Boon, M.E. Microwaves for Microscopy. *J Microsc* **1990**, *158*, 291–322, doi:10.1111/j.1365-2818.1990.tb03003.x.
22. Giberson, R.T.; Demaree, R.S.J. Microwave Processing Techniques for Electron Microscopy: A Four-Hour Protocol. *Methods Mol Biol* **1999**, *117*, 145–158, doi:10.1385/1-59259-201-5:145.
23. Giberson, R.T.; Austin, R.L.; Charlesworth, J.; Adamson, G.; Herrera, G.A. Microwave and Digital Imaging Technology Reduce Turnaround Times for Diagnostic Electron Microscopy. *Ultrastruct Pathol* **2003**, *27*, 187–196, doi:10.1080/01913120309937.
24. Webster, P. Microwave-Assisted Processing and Embedding for Transmission Electron Microscopy. *Methods Mol Biol* **2014**, *1117*, 21–37, doi:10.1007/978-1-62703-776-1_2.
25. Russell, M.R.G.; Lerner, T.R.; Burden, J.J.; Nkwe, D.O.; Pelchen-Matthews, A.; Domart, M.-C.; Durgan, J.; Weston, A.; Jones, M.L.; Peddie, C.J.; et al. 3D Correlative Light and Electron Microscopy of Cultured Cells Using Serial Blockface Scanning Electron Microscopy. *J Cell Sci* **2017**, *130*, 278–291, doi:10.1242/jcs.188433.
26. Schauflinger, M.; Villinger, C.; Walther, P. Three-Dimensional Visualization of Virus-Infected Cells by Serial Sectioning: An Electron Microscopic Study Using Resin Embedded Cells. *Methods Mol Biol* **2013**, *1064*, 227–237, doi:10.1007/978-1-62703-601-6_16.